Block of Voltage-Dependent Calcium Channels by Aliphatic Monoamines

Aaron M. Beedle and Gerald W. Zamponi
Department of Pharmacology and Therapeutics, University of Calgary, Calgary, Alberta T2N 4N1, Canada

ABSTRACT   We have recently identified farnesol, an intermediate in the mevalonate pathway, as a potent endogenous modulator and blocker of N-type calcium channels (Roullet, J. B., R. L. Spaetgens, T. Burlingame, and G. W. Zamponi. 1999. *J. Biol. Chem.* 274:25439–25446). Here, we investigate the action of structurally related compounds on various types of voltage-dependent Ca^{2+} channels transiently expressed in human embryonic kidney cells. 1-Dodecanol, despite sharing the 12-carbon backbone and headgroup of farnesol, exhibited a significantly lower blocking affinity for N-type Ca^{2+} channels. Among several additional 12-carbon compounds tested, dodecylamine (DDA) mediated the highest affinity inhibition of N-type channels, indicating that the functional headgroup is a critical determinant of blocking affinity. This inhibition was concentration-dependent and relatively non-discriminatory among N-, L-, P/Q-, and R-Ca^{2+} channel subtypes. However, whereas L-type channels exhibited predominantly resting channel block, the non-L-type isoforms showed substantial rapid open channel block manifested by a speeding of the apparent time course of current decay and block of the inactivated state. Consistent with these findings, we observed significant frequency-dependence of block and dependence on external Ba^{2+} concentration for N-type, but not L-type, channels. We also systematically investigated the drug structural requirements for N-type channel inhibition. Blocking affinity varied with carbon chain length and showed a clear maximum at C12 and C13, with shorter and longer molecules producing progressively weaker peak current block. Overall, our data indicate that aliphatic monoamines may constitute a novel class of potent inhibitors of voltage-dependent Ca^{2+} channels, with block being governed by rigid structural requirements and channel-specific state dependencies.

INTRODUCTION

Calcium entry through voltage-gated channels mediates a variety of physiological responses such as muscle contraction, control of pacemaker activity, neurotransmitter release, activation of Ca^{2+}-dependent proteins, and induction of gene transcription (e.g., McCleskey, 1994; Dickson et al., 1997; Lemos and Nowycky, 1989; Higuchi et al., 1996). Consequently, Ca^{2+} channels are important pharmacological targets in designing treatments for cardiac arrhythmias, stroke, migraine, cerebellar ataxia, and some forms of epilepsy (e.g., Camm et al., 1991; Ophoff et al., 1996; Fletcher et al., 1996). Thus, it is of importance to understand the molecular determinants governing the interactions between drugs and the channel protein, and it is desirable to identify novel classes of compounds that interact with these channels.

Neuronal Ca^{2+} channels are heteromultimers of α_1, α_2, β, and δ subunits. The α_1 subunit, consisting of four repeat domains of six transmembrane helices and a P-loop, provides the pore, voltage sensor, and inactivation machinery of the channel (Catterall, 1991). To date, as many as 10 α_1 subunit genes have been identified, which are classified into the low voltage-activated (LVA) T-type channels and the high voltage-activated (HVA) N-, L-, P-, Q-, and R-types based on diverse biophysical and pharmacological properties (for review, see Tsien et al., 1991; Zhang et al., 1993).

α_{1C}, α_{1D}, α_{1F}, and α_{1S} encode L-type Ca^{2+} channels (Tomlinson et al., 1993; Williams et al., 1992b; Bech-Hansen et al., 1998; Ellis et al., 1988), α_{1A} makes P/Q-type channels through alternative splicing (Bourinet et al., 1999), α_{1B} gives rise to N-type channels (Williams et al., 1992a), α_{1E} is a unique type with characteristics common to both LVA and HVA channels (Williams et al., 1994), and α_{1G}, α_{1H}, and α_{1I} encode T-type Ca^{2+} channels (Perez-Reyes et al., 1998; Cribbs et al., 1998; Lee et al., 1999). The α_1 subunit is the target for most of the known Ca^{2+} channel blockers (for review, see Zamponi, 1997), and the particular pharmacological profile is frequently used as a key characteristic to help identify a given Ca^{2+} channel subtype. For example, ω-conotoxins GVIA and MVIIA are specific for the α_{1B} subunit (e.g., Boland et al., 1994; Fox, 1995), ω-agatoxin IVA is selective for α_{1A} (e.g., Mintz et al., 1992), and dihydropyridines are specific blockers of the L-type isoforms (e.g., Bangalore et al., 1994). In addition, there are many types of far less selective Ca^{2+} channel blockers that may reflect the overall degree of homology among individual Ca^{2+} channel subtypes (i.e., Zamponi, 1997).

Recently, we have shown that farnesol, an intermediate of the mevalonate pathway, mediates both a selective high affinity (100 nM) inhibition of inactivated α_{1B} channels and a non-selective lower affinity (5–10 μM) resting/open channel block of all types of HVA channels (Roullet et al., 1999). Here, we examine the action of a series of commercially available farnesol analogs on Ca^{2+} channels transiently expressed in human embryonic kidney (HEK) cells. Among several 12 carbon chain molecules tested, dodecylamine (DDA) was identified as a highly potent inhibitor of HVA channels. Qualitatively similar to farnesol, DDA

caused a nonselective peak current inhibition of all types of Ca^{2+} channels tested, with block of the L-type channels differing from that of non-L-type isoforms in its state-dependence, use-dependence, and dependence on the external permeant ion concentration. Experiments with a series of additional aliphatic monoamines differing only in carbon chain length revealed strict drug structural requirements for N-type channel inhibition, with maximum inhibition occurring at a chain length of 13 carbons. Overall, our data show that remarkably simple small organic molecules may have the propensity to potently inhibit neuronal calcium channels.

MATERIALS AND METHODS

Materials

Rat brain cDNAs coding for α_{1A}, α_{1B}, α_{1C}, α_{1E}, and α_2-δ were donated by Dr. T. P. Snutch (University of British Columbia). The following compounds were obtained from Sigma (St. Louis, MO): n-nonylamine, n-decylamine, DDA, n-dodecane; Aldrich (Milwaukee, WI): tridecylamine, 1-tetradecylamine, pentadecylamine, 1-hexadecylamine, octadecylamine, 1-dodecanol, 4-dodecylphenol (mixture of isomers), dodecylacetate; and Acros (New Jersey, NJ): n-undecylamine. Drugs were stored as 100 mM stock solutions in 100% ethanol and diluted into the appropriate external recording solutions at the final concentrations necessary. The final ethanol concentrations in the drug solutions ($\leq$0.01%), when tested alone, have previously been shown to have no effect on calcium channel currents (Roullet et al., 1999).

Cell culture and transient transfection of HEK cells

HEK tSA 201 cells were cultured in Dulbecco's modified Eagle's medium (DMEM) supplemented with 10% fetal bovine serum, 200 U/ml penicillin, and 0.2 mg/ml streptomycin at 37°C with 5% CO$_2$. At 85% confluency, cells were split with 0.25% trypsin-1 mM EDTA and plated at 10% confluency on glass coverslips. At 12 h, medium was replaced and cells were transiently transfected, using a standard calcium phosphate protocol, with cDNAs encoding calcium channel α_1, α_2-δ, and β_{1b} subunits and green fluorescent protein (EGFP, Clontech) at a 3:3:3:2 ratio. Fresh DMEM was supplied and cells were moved to 28°C, 5% CO$_2$ at 12 and 24 h after transfection, respectively. Cells were stored 1–2 days before recording. All tissue culture reagents were obtained from Life Technologies, Inc. (Grand Island, NY).

Electrophysiological recordings and analysis

Voltage-clamp data acquired using pClamp version 6.0.3 software (Axon Instruments, Foster City, CA) were filtered at 1 kHz via an Axopatch 200B amplifier (Axon Instruments) and stored on an IBM-compatible PC. Borosilicate glass patch pipettes (Sutter Instrument Co., Novato, CA) were polished (Microforge, Narishige, Japan) to a resistance of ~4 MΩ when filled with cesium methanesulfonate internal solution (composition in mM: 109 CsCH$_3$SO$_4$, 4 MgCl$_2$, 9 EGTA, 9 HEPES, pH 7.2). Cells were bathed in external solution containing either 20 mM BaCl$_2$, 1 mM MgCl$_2$, 10 mM HEPES, 40 mM tetraethylammonium chloride, 10 mM glucose, 65 mM CsCl (pH 7.2) or 2 mM BaCl$_2$, 1 mM MgCl$_2$, 10 mM HEPES, 40 mM tetraethylammonium chloride, 10 mM glucose, 105 mM CsCl (pH 7.2). Unless stated otherwise, current data shown were elicited by a 0.066 Hz train of 100-ms test pulses from $-$100 mV to various potentials (min. $-$20 mV, max. $+$30 mV). Drugs were perfused directly into the vicinity of the cells using a home-built microperfusion system capable of solution exchanges in less than one second.

Data were analyzed using Clampfit 6.0 (Axon Instruments). The time constant of current decay was measured at various DDA concentrations by exponential fits to the raw data. The control decay rate was fit with a single exponential with time constant τ_h, while currents in the presence of DDA were fit with a double exponential with one of the time constants fixed at the control τ_h value. The inverse of τ was then plotted as a function of DDA concentration. Assuming a 1:1 open channel blocking interaction, $1/\tau = [D]k_{on} + k_{off}$, where [D] is the drug concentration and k_{on} and k_{off} are, respectively, the blocking and unblocking rate constants.

Normalized dose-response curves were fit (SigmaPlot 4.0, SPSS Inc., Chicago, IL) by the Hill equation to determine IC$_{50}$ values. Steady-state inactivation curves were plotted as the normalized test pulse amplitude following 5-s inactivating prepulses in 10-mV increments. Inactivation curves were fit (SigmaPlot 4.0) with the Boltzmann equation, I_{peak} (normalized) $= 1/(1 + \exp((V - V_h)z/25.6))$, where V and V_h are the conditioning and half-inactivation potentials, respectively, and z is the slope factor. All error bars show standard error of the mean; any numbers in parentheses shown in a figure reflect the numbers of experiments, and p values reflect paired or Student's t-tests.

RESULTS

An amine headgroup enhances N-type calcium channel block by linear C12 compounds

We have previously shown that farnesol mediates a high affinity modulation of inactivated N-type calcium channels and a lower affinity non-selective block of all types of neuronal HVA calcium channels (Roullet et al., 1999). To elucidate some of the underlying drug structural requirements, we examined the effects of several commercially available farnesol derivatives on transiently expressed N-type calcium channels (bathed in 20 mM Ba^{2+}), and compared them to those previously observed with farnesol. Like farnesol, 1-dodecanol (see Fig. 1) exhibits a C12 hydrocarbon chain backbone and an alcohol group; however, the double bonds and three methyl groups of farnesol are lacking. At a concentration of 10 μM and a holding potential of $-$100 mV, 1-dodecanol caused a 14 $\pm$ 2% inhibition of peak current amplitude of N-type calcium channels. This was significantly lower than that observed with farnesol (38 $\pm$ 4%), indicating that either the more rigid double bonds or the added hydrophobicity associated with the three methyl groups in farnesol serve to enhance blocking affinity. To examine a putative role of the alcohol group for calcium channel block, we then varied the functional group attached to the dodecyl backbone (see Fig. 1). Whereas 10 μM n-dodecane, 4-dodecylphenol, and dodecylacetate failed to produce more than about a 15% inhibition of peak current amplitude, application of 10 μM DDA virtually completely (97 $\pm$ 1%) eliminated the N-type currents (Fig. 1 *B*). Thus, the addition of an amine headgroup to the dodecyl backbone structure mediated an almost 30-fold increase in blocking affinity, well exceeding that observed originally with farnesol. These data indicate that the functional group attached to the dodecyl backbone is a critical determinant of blocking affinity, and that aliphatic mono-
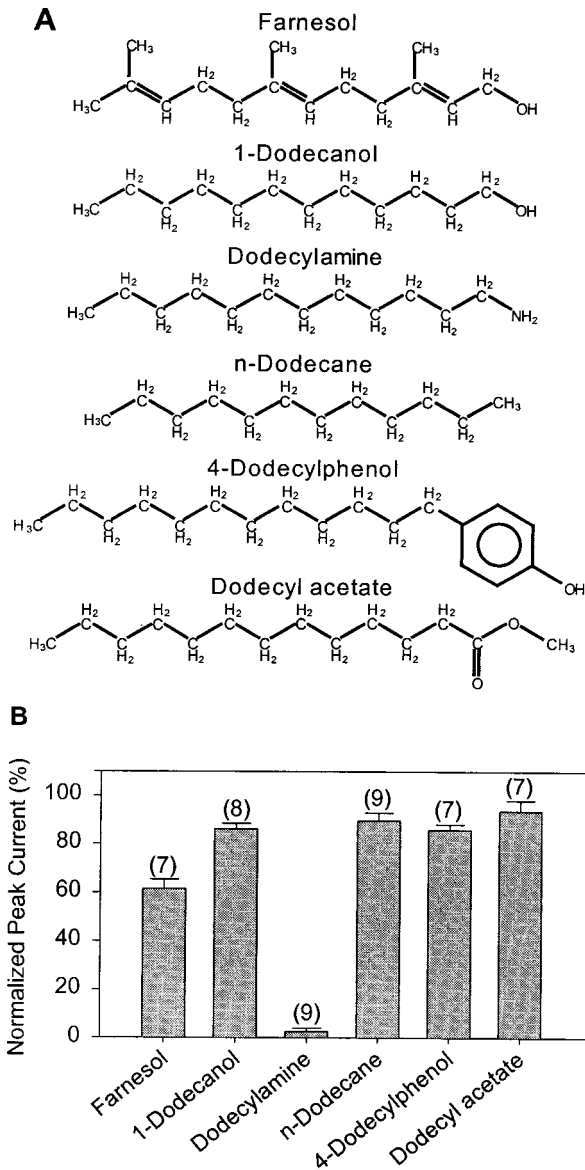
A

B

FIGURE 1 Peak current block of N-type calcium channels by farnesol analogs. (*A*) Chemical structures of farnesol and a series of derivatives with a C12 backbone. Note that these farnesol analogs differ only in their functional groups. (*B*) Effect of application of 10 μM concentrations of the compounds depicted in *A* on N-type (α_{1B} + α_2-δ + β_{1b}) currents carried by 20 mM barium. Currents were elicited by stepping from −100 mV to +10 mV at 15-s intervals. The data are plotted as peak current remaining after drug application. Note that dodecylamine (DDA) mediates the most pronounced inhibition of N-type channels. Current remaining: farnesol, 62 ± 4%; 1-dodecanol, 86 ± 2%; DDA, 3 ± 1%; n-dodecane, 90 ± 3%; 4-dodecylphenol, 86 ± 2%; and dodecylacetate, 94 ± 4%. Numbers in parentheses indicate the numbers of experiments, the error bars reflect standard errors.

amines have the propensity to potently block voltage-dependent calcium channels. To further characterize the action of DDA, and to test whether the basic blocking properties previously observed with farnesol were preserved with the

structurally simpler DDA, we carried out a detailed characterization of DDA block on four different types of high voltage-activated calcium channels.

DDA mediates both resting and open channel block

In order to test for a putative calcium channel isoform selectivity of DDA block, α_{1A}, α_{1B}, α_{1C}, and α_{1E} channels (coexpressed with β_{1b} and α_2-δ in tSA-201 cells) were exposed to various concentrations of DDA. Fig. 2 *A* shows representative current traces for each of the channel subtypes bathed in 20 mM Ba^{2+}. In all cases, DDA induced a reversible reduction in peak current amplitude, with α_{1C} exhibiting the most pronounced inhibition as evident by comparing the effect of 3 μM DDA on the current traces. This is also reflected in the dose-response curves depicted in Fig. 2 *B*. The IC_{50} values obtained from the fits were, respectively, 0.8 μM, 1.8 μM, 2.0 μM, and 2.1 μM for α_{1C}, α_{1B}, α_{1E}, and α_{1A}, indicating a two to threefold higher affinity for L-type compared to non-L-type channels, but overall a poor selectivity among individual calcium channel subtypes. For all channel types examined, the inhibition of peak current amplitude exhibited little if any detectable dependence on test potential (not shown).

Similar to what we had previously observed with farnesol, DDA mediated a speeding of the apparent time course of inactivation. If DDA binding simply speeds inactivation of the channel, the drug-bound channels would inactivate with the faster rate, whereas the non-bound channels would inactivate normally, thus yielding a double-exponential macroscopic decay rate. With increasing drug concentrations, the proportion of the drug-bound channels, and thus the contributions of the faster inactivation time constants to the overall inactivation rate, would increase, but the absolute values of the two time constants should remain independent of DDA concentration. In contrast, if the speeding were due to open channel block developing during the test depolarization, the rate of development of block, and thus the DDA-induced second time constant, would be expected to depend inversely on DDA concentration. To discriminate between these two alternatives, the time course of current decay in the presence of various DDA concentrations was fit with two exponentials (τ and τ_h), where τ_h was fixed at the value obtained in the absence of DDA (see Methods). As seen from Fig. 2 *C*, the inverse of the DDA-induced second time constant (τ) increased linearly with DDA concentration, consistent with the open channel blocking model and our previous observations with farnesol (Roullet et al., 1999). In this scenario, the slope and *y*-intercept of the regression line would reflect the blocking and unblocking rate constants, respectively (see Methods). As seen from Fig. 2 *C*, block of the three non L-type channels occurred with similar kinetics, whereas L-type channels exhibited
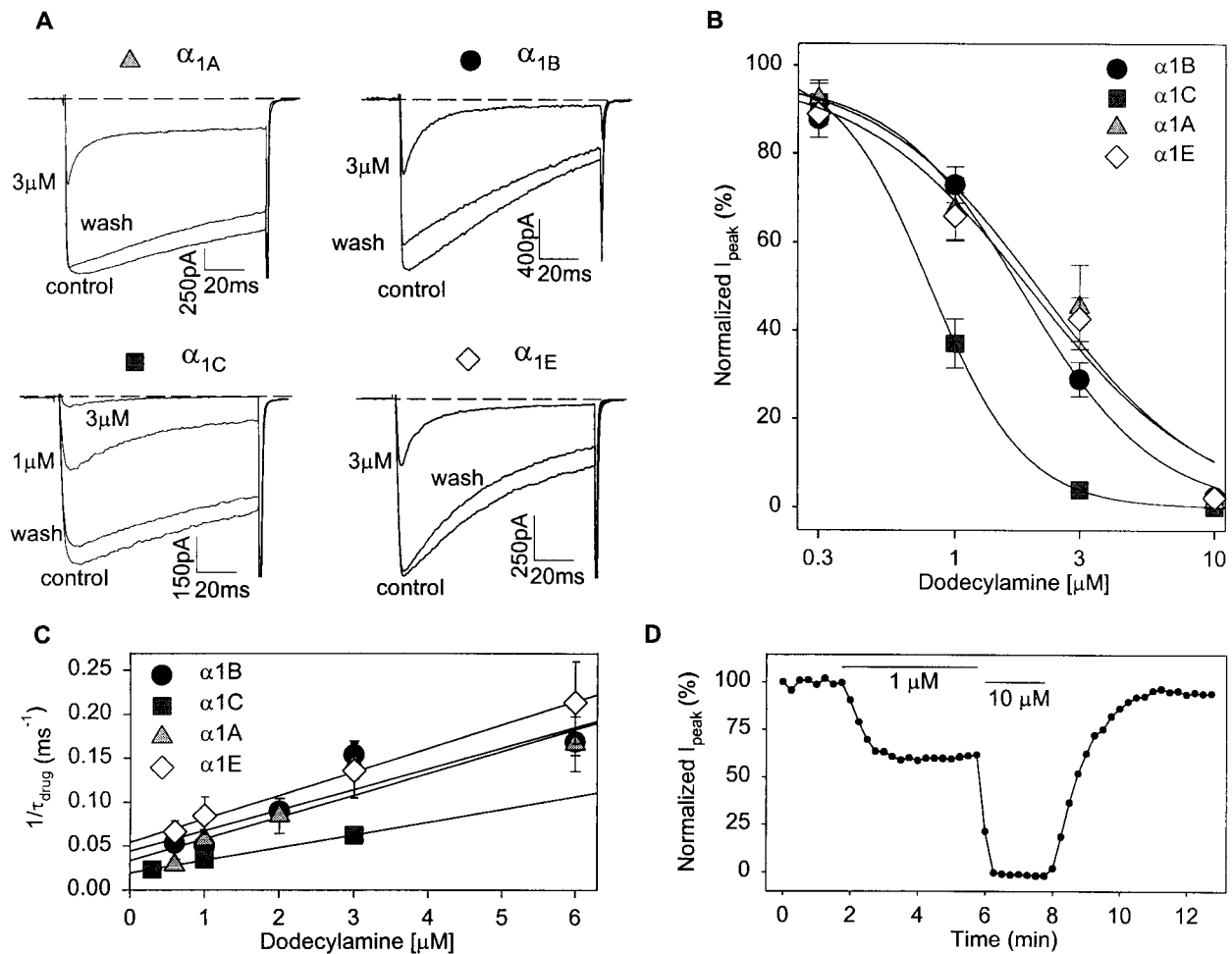
FIGURE 2 Comparison of DDA effects on various types of calcium channels. (A) Current records obtained for four Ca^{2+} channel subtypes. Currents were evoked as described for Fig. 1, the external barium concentration was 20 mM. All subtypes showed reversible peak current inhibition by 3 μM DDA. Note an apparent speeding of inactivation is also evident in α_{1A}, α_{1B}, and α_{1E}, and to a smaller degree, in α_{1C} current traces. (B) Comparison of dose-dependence of peak current inhibition of HVA calcium channels by DDA. Data were plotted as peak current mean $\pm$ SEM and fit with the Hill equation. Each data point reflects between 6 and 10 determinations. α_{1C} was most sensitive to DDA with an IC$_{50}$ of 0.8 $\pm$ 0.1 μM (n_h = 2.4) followed by α_{1B}, α_{1E}, and α_{1A} at 1.8 $\pm$ 0.2 (n_h = 1.7), 2.0 $\pm$ 0.2 (n_h = 1.3), and 2.1 $\pm$ 0.6 μM (n_h = 1.4), respectively. (C) Kinetic analyses of the dose-dependent increase in the rate of apparent current decay with DDA for each calcium channel tested. Current records were fit as described in the Methods, and the DDA-induced time constant τ was plotted as a function of DDA concentration. Plots were fit with the linear regression equation $1/\tau = k_{off} + k_{on}[\text{DDA}]$. The values obtained from the fits were as follows: α_{1A}, k_{on} = 0.024 μM^{-1} ms^{-1}, k_{off} = 0.023 ms^{-1}; α_{1B}, k_{on} = 0.023 μM^{-1} ms^{-1}, k_{off} = 0.0443 ms^{-1}; α_{1C}, k_{on} = 0.014 μM^{-1} ms^{-1}, k_{off} = 0.019 ms^{-1}; and α_{1E}, k_{on} = 0.0265 μM^{-1} ms^{-1}, k_{off} = 0.0546 ms^{-1}. (D) Time course of α_{1B} current inhibition by DDA. The normalized α_{1B} peak current elicited by consecutive step pulses to +10 mV was plotted showing control, 1 μM DDA, 10 μM DDA, and wash responses. The magnitude of block and the rate of block development increased with the higher DDA concentration as expected, and the effect was fully reversible. Note that the block by 1 μM DDA reached equilibrium within two minutes, the equilibration time used for steady-state inactivation and frequency-dependence experiments (see below).

about twofold slower blocking and unblocking rate constants. Overall, these data may indicate that the open channel blocking site is highly conserved across different types of voltage-dependent calcium channels. For each of the channels examined, open channel block could account for only part of the overall inhibition observed at the time of peak, thus suggesting the presence of an additional tonic (i.e., resting channel) blocking component. Among the four channel types examined, the L-type isoform was subject to

the largest contribution from resting block, which could account for nearly 90% of the peak current reduction observed in the presence of 1 μM DDA. A substantial contribution from resting channel block was also observed with α_{1B}, which contrasts with our previous observations with farnesol, where the peak current inhibition of α_{1B} could be attributed almost exclusively to open channel block developing during the activation phase (Roullet et al., 1999). In contrast, the inhibition seen at the end of the test depolar-

ization is predominantly due to open channel block, with some contribution from the initial tonic block.

The kinetic analysis depicted in Fig. 2 *C* suggests that after drug equilibration, block and unblock of the channels occurs in the range of milliseconds. This contrasts with the much slower time course of development of, and recovery from, peak current inhibition of α_{1B} evident in Fig. 2 *D*, which occurred over the course of one to two minutes. Thus, similar to what we had observed, with farnesol, DDA block of HVA calcium channels appears to involve a rate-limiting step other than the true interaction rates between the blocker and the channel, such as partitioning into the plasma membrane.

DDA mediates inactivated channel block of non-L-type channels

One of our key observations with farnesol was a selective inhibition of inactivated N-type calcium channels (Roullet et al., 1999) demonstrated by a farnesol-mediated shift in half-inactivation potential. To test whether DDA could mediate a similar inhibition, we investigated the effect of 1 μM DDA on the position of the steady-state inactivation curves of the four types of calcium channels with 20 mM barium as the external charge carrier. As evident from Fig. 3, DDA

mediated a 10–15-mV shift in half-inactivation potential for all of the non-L-type channels tested. Thus, unlike farnesol, inactivated channel block by DDA is not exclusive to N-type calcium channels. These observations might indicate that the double bonds and/or the additional methyl side chains of farnesol (see Fig. 1) could contribute to the N-type channel selectivity of inactivated channel block. Whereas the shifts in half-inactivation potential observed with non-L-type channels do not significantly affect peak current levels at hyperpolarized holding potentials (i.e., −100 mV, such as in Fig. 2), at a typical neuronal resting potential (i.e., −70 mV), these shifts in the midpoint of the steady-state inactivation curve would result in further depression of peak current amplitude in addition to that mediated by open and resting channel block. In contrast with non-L-type channels, application of 1 μM DDA did not significantly affect the position of the steady-state inactivation curve of α_{1C}, indicating that L-type channels do not undergo inactivated channel block.

We also tested the effects of 1-dodecanol on the steady-state inactivation of α_{1B}. As in the case of DDA, a 12 mV negative shift in half-inactivation potential was observed (not shown), however, only at 10-fold higher concentrations (10 μM), whereas application of 1 μM 1-dodecanol was ineffective. Together with our previous observation with
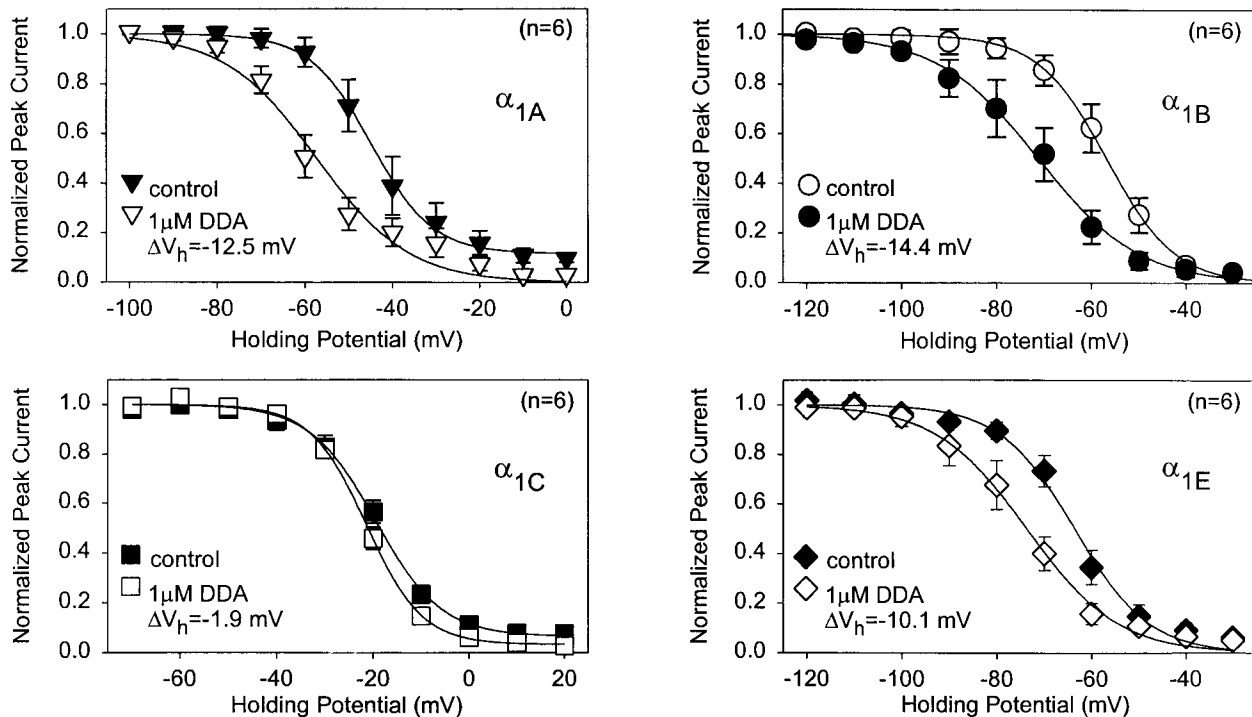

FIGURE 3   DDA induces a hyperpolarizing shift in the steady-state inactivation curves of non-L-type channels. Steady-state inactivation curves were acquired by holding the cells at various conditioning potentials for 5 s prior to stepping to +10 mV. 1 μM DDA induced a 10 mV to 15 mV hyperpolarizing shift in inactivation for α_{1A} (control $V_h = -44.8 \pm 0.5$ mV, $z = 3.7$; 1 μM $V_h = -57.3 \pm 1.3$ mV, $z = 2.5$), α_{1B} (control $V_h = -56.8 \pm 0.3$ mV, $z = 3.56$; 1 μM $V_h = -71.2 \pm 0.6$ mV, $z = 2.44$), and α_{1E} (control $V_h = -63.6 \pm 0.8$ mV, $z = 3.2$; 1 μM $V_h = -73.7 \pm 0.7$ mV, $z = 2.7$). DDA did not significantly affect the half-inactivation potential of α_{1C} L-type channels (control $V_h = -19.5 \pm 0.4$ mV, $z = 3.7$; 1 μM $V_h = -21.4 \pm 0.3$ mV, $z = 4.4$). The external barium concentration was 20 mM.

farnesol, where a shift of similar magnitude was observed at concentrations as low as 100 nM (Roullet et al., 1999), these data indicate that the functional group on the dodecyl backbone and the actual backbone structure contribute to the affinity for the inactivated state of N-type channels.

DDA block of L-type and N-type channels differs in its use-dependence

From the observation that L-type calcium channels predominantly exhibit resting channel block, whereas the non-L-

type isoforms also show substantial inactivated and open channel block, one might predict a selective use-dependence of DDA action on non-L-type channels. Under control conditions with α_{1B} or α_{1C} (*open symbols*, Fig. 4, *C* and *D*), increasing the pulse frequency mediated only a small (<5%) degree of current inhibition, indicating that little inactivation accumulates in the absence of DDA even at the highest pulse frequency (2 Hz) used. Fig. 4, *A* and *B* depict the effect of a 2 Hz stimulation on current levels before (*left traces*) and after complete (2 min) equilibration (*right traces*) with DDA. Under those conditions, the first test
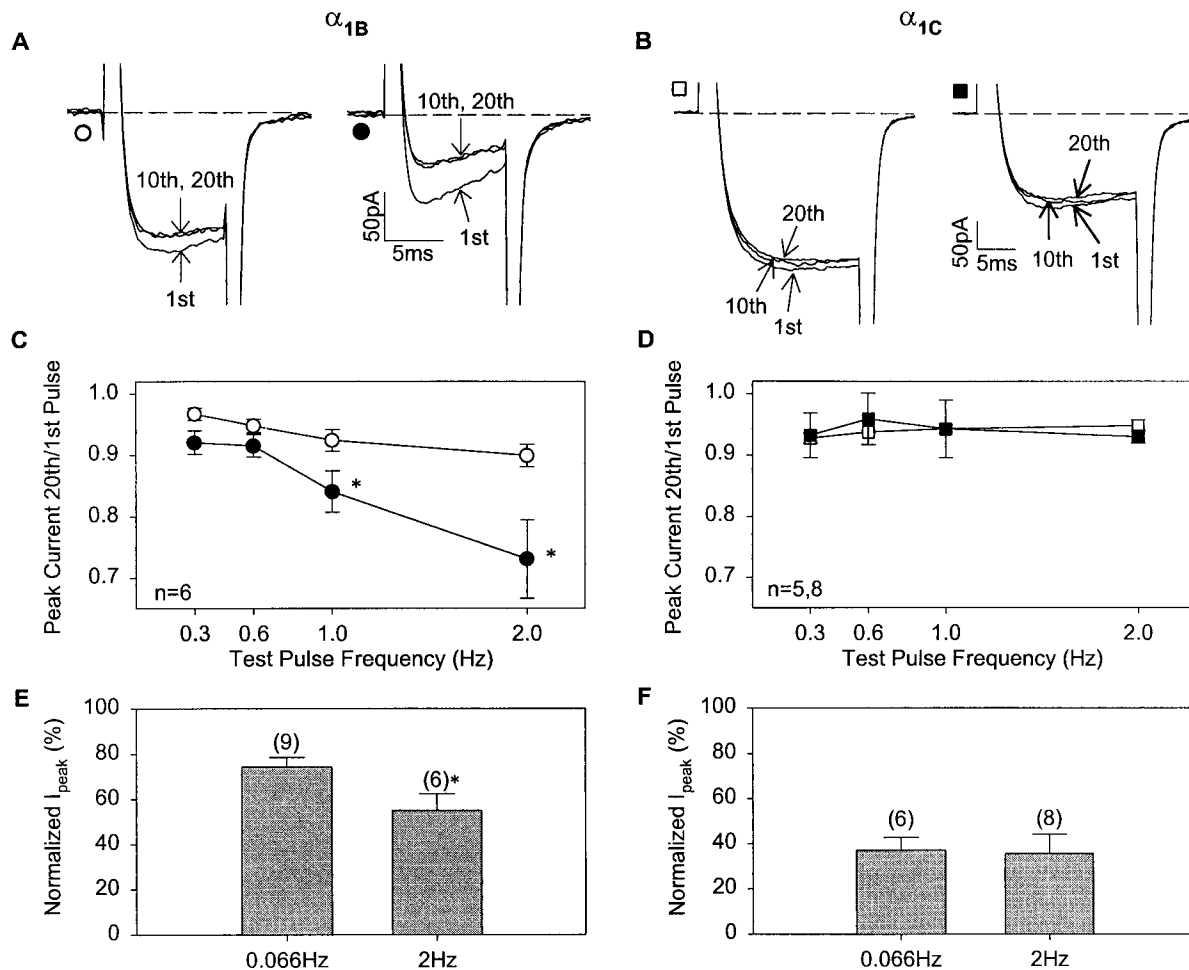

FIGURE 4 Frequency-dependence of DDA block. Frequency protocols consisted of 20 test pulses from -100 mV to various potentials at 0.3, 0.6, 1.0, or 2.0 Hz. Protocols were administered in random order and followed by 60-s recovery periods. One μM DDA was applied 30 s after the last frequency protocol in control conditions and allowed to equilibrate for 2 min prior to resumption of the pulse protocol. (*A* and *B*) Representative current traces of the 1st, 10th, and 20th steps of a 2 Hz protocol for N-type (α_{1B}, α_2-δ, β_{1b}) and L-type (α_{1C}, α_2-δ, β_{1b}) calcium channels, respectively. Left traces show control currents and right traces were recorded in the presence of 1 μM DDA. Scale bars apply to both left and right traces, all experiments were performed in 20 mM external barium. Note that additional block of N-type channels developed during the train, whereas L-type channels did not undergo further inhibition after the first pulse. (*C* and *D*) Frequency-dependence plots in control (*open symbols*) and 1 μM DDA (*filled symbols*) conditions for α_{1B} and α_{1C}. Data are plotted as the ratio between the current amplitudes obtained at the 20th and the 1st pulse for each frequency train, under both control and DDA conditions. Data were tested for significant differences between control and DDA data via paired t-tests (*$p < 0.05$). DDA induced significant frequency-dependence at both 1 ($p = 0.03$) and 2 Hz ($p = 0.02$) frequencies. (*E* and *F*) Comparison of total block by 1 μM DDA as measured by the original step protocol at 0.066 Hz (see Fig. 2) and the frequency-dependence protocol at 2 Hz. Data are plotted as the ratio of the peak current amplitudes obtained at the 20th step in the absence and the presence of DDA. Block by DDA as measured by the 2 Hz protocol was significantly different from block at 0.066 Hz of α_{1B} (t-test, $p = 0.03$) but not α_{1C} currents (α_{1B}: 0.066 Hz $I_{peak} = 25.6 \pm 4.3\%$, 2 Hz $I_{peak} = 45.0 \pm 7.3\%$; α_{1C}: 0.066 Hz $I_{peak} = 62.8 \pm 5.6\%$, 2 Hz $I_{peak} = 64.4 \pm 8.5\%$).

pulse in the train after drug equilibration reveals tonic peak current block of, respectively, $20 \pm 5\%$ and $48 \pm 6\%$ for α_{1B} and α_{1C}. As the train continues, significant use-dependent block develops for α_{1B}, but not for α_{1C}. This can be seen upon comparison of the current levels obtained during the 1st, 10th, and 20th pulses in the train and is further illustrated in Fig. 4, *C* and *D* for a series of different pulse train frequencies. As evident from the figure, α_{1B}, but not α_{1C}, channels accumulated a significant additional block at 1 and 2 Hz stimulus rates compared with slower rates of stimulation. Fig. 4, *E* and *F* compare total peak current amplitude inhibition by DDA in the 2 Hz pulse protocol and the original (0.066 Hz) step protocol used in Fig. 2 *B*. Besides the open channel and tonic blocking components described earlier, higher frequency stimulation produced an additional 20% block of α_{1B} channels, whereas α_{1C} channels were not significantly affected. The lack of use-dependence observed with α_{1C} is consistent with the idea that these channels undergo predominantly resting channel block. Overall, our data further support the notion that L-type channel block by DDA differs from that of non-L-type channels in its state-dependence.

DDA block of L-type and N-type channels differs in its sensitivity to [Ba]$_o$

We have previously hypothesized that open channel block by farnesol might occur via physical occlusion of the pore (Roullet et al., 1999). One feature frequently associated with pore block is a dependence of blocking affinity on the concentration of external carrier ion. To test whether such a characteristic could be observed with DDA, we reduced the concentration of external permeant ion from 20 mM to 2 mM and assessed the change in blocking affinity for N-type and L-type channels. Fig. 5, *A* and *B* depict the effects of DDA in the form of representative current traces obtained in 20 mM (from Fig. 2 *A*) and 2 mM external barium solutions. For α_{1B}, the degree of peak current inhibition by DDA was dramatically enhanced in 2 mM barium. Furthermore, in lower external saline, the speeding of the time course of current decay was observed at lower DDA concentrations, consistent with our interpretation that the enhanced decay rate in the presence of DDA reflected open channel block. Analysis of the rate of current decay in 2 mM barium solution revealed a 52% increase in the association rate
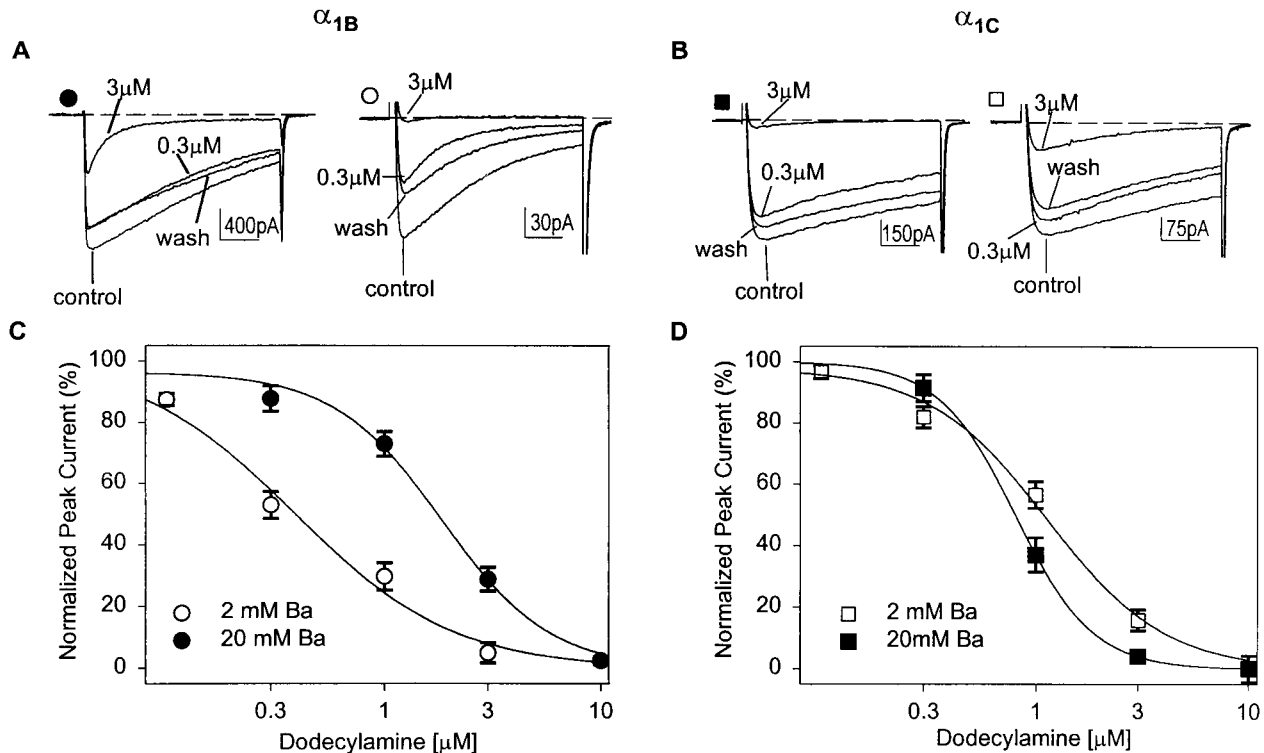

FIGURE 5   Selective dependence of N-type channel block by DDA on the concentration of external barium ions. DDA block of α_{1B} and α_{1C} was assessed in either 2 mM or 20 mM external barium solution using a step protocol from -100 mV to $+10$ mV. (*A* and *B*) Representative current traces of DDA block in 20 mM (*filled symbols*) and 2 mM (*open symbols*) external barium solution for α_{1B} and α_{1C}, respectively. The magnitude of the vertical scale bar is indicated for each trace; all horizontal scale bars reflect 20 ms. Note that N-type channels become more sensitive to DDA in lower external saline. (*C* and *D*) Dose-response curves for DDA block under both external barium concentrations were fit with the Hill equation. Individual data points are means from 4 to 10 determinations. The data obtained in 20 mM barium are the same as those shown in Fig. 2 *B*. α_{1B} currents were blocked with IC$_{50}$ values of 1.8 ± 0.2 μM for 20 mM barium ($n_h = 1.7$) and 0.4 ± 0.1 μM for 2 mM barium solution ($n_h = 1.2$). Alternately, α_{1C} currents showed IC$_{50}$ values of 0.8 ± 0.1 μM ($n_h = 2.4$) and 1.1 ± 0.1 μM ($n_h = 1.6$) in 20 mM and 2 mM external barium, respectively.

constant (k_{on}) and a 12% decrease in the dissociation rate constant (k_{off}) compared to 20 mM barium, indicating a slightly less than twofold increase in blocking affinity in lower external barium solution. In contrast, α_{1C} currents actually underwent, if anything, a slight decrease in blocking affinity when external barium was reduced to 2 mM. This is further illustrated in form of dose-response curves (Fig. 5, C and D) for peak current inhibition. Whereas reduction of external charge carrier concentration had little effect on α_{1C} channels, the IC$_{50}$ for DDA block of α_{1B} was decreased approximately fivefold. In view of the relatively moderate effects of charge carrier concentration on the open channel blocking affinity, the larger effect observed with the dose-dependence of peak current inhibition of α_{1B} channels may suggest that both open and resting channel block were affected, which cannot easily be explained by a simple competition between barium ions and DDA within the permeation pathway. Thus, there appears to be a fundamental difference in the detailed mechanism by which DDA mediates peak current block of N-type and L-type channels. Finally, of particular note, with an IC$_{50}$ of ~400 nM in 2 mM Ba^{2+}, DDA is among the most potent small organic inhibitors of N-type channel activity described to date, which is remarkable in view of the structural simplicity of the compound.

Blocking affinity for N-type channels depends on hydrocarbon chain length

To examine whether block of N-type calcium channels by aliphatic monoamines might be dependent on the length of the hydrocarbon backbone, we systematically varied the backbone chain length while keeping the functional amine headgroup constant. Eight additional commercially available aliphatic monoamines ranging in chain length from 9 to 18 carbons were tested on N-type calcium channels bathed in 20 mM barium saline at a holding potential of −100 mV. Fig. 6 illustrates peak current block by each of these compounds at a concentration of 10 μM. A pattern of chain length-dependence is readily observable. C12 (DDA) and C13 (tridecylamine) abolished virtually all of the current. With decreasing hydrocarbon chain length, blocking affinity became progressively reduced from 73 ± 7% block (C11) to 21 ± 3% block (C9). Likewise, as chain length was increased, the degree of N-type channel block decreased monotonically to 7 ± 3% for C18. Overall, it appears as if a chain length of 12 or 13 carbons yields optimum conditions for N-type channel block. Thus, the three-dimensional makeup of the drug binding site on the N-type calcium channel molecule appears to place strict physical constraints on the size of drug molecule it can accommodate, which in turn may provide insights into the pore structure.
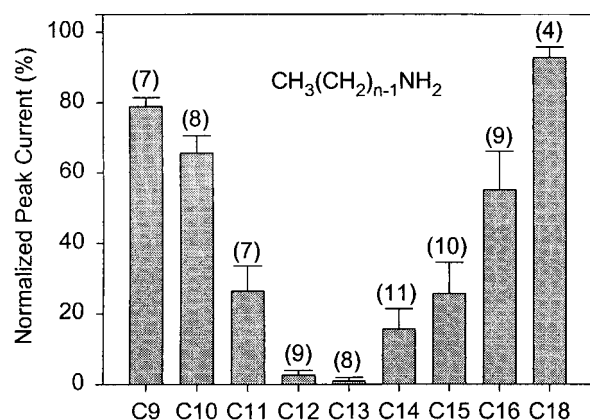

FIGURE 6 Block of transiently expressed (α_{1B} + $\alpha_{2\text{-}\delta}$ + β_{1b}) N-type calcium channels by aliphatic monoamines is dependent on hydrocarbon chain length. All compounds were applied at a concentration of 10 μM in 20 mM external barium solution using a standard step protocol (holding potential −100 mV, test potential +10 mV). Cn indicates the length of the hydrocarbon backbone for each of the amines. The data are plotted as the percentage of current remaining after drug application. Blocking affinity was greatest for DDA (C12; current remaining 2.7 ± 1.3%) and tridecylamine (C13, current remaining 1.0 ± 1.0%) with decreasing effect as hydrocarbon chain length was either increased or decreased.

DISCUSSION

Comparison with farnesol block

In our previous study on farnesol, we demonstrated that farnesol caused two types of inhibition of voltage-dependent calcium channels: a low affinity inhibition that showed a slight preference for L-type channels, but was nonetheless relatively nonselective for different types of HVA channels, and a higher affinity inactivated channel block that was selective for N-type channels (Roullet et al., 1999). There are three major structural differences between DDA and farnesol (see Fig. 1), as DDA lacks the three double bonds and methyl groups in the backbone, and the terminal -OH group of farnesol is replaced by an amine. It is perhaps not surprising to note that DDA action differed from that of farnesol in several ways. First, DDA block (at a holding potentials of −100 mV) occurred with 10-fold higher affinity. Second, while this type of inhibition retained a slight preference for L-type channels, the contribution of resting channel block to the overall peak current block seen with non-L-type channels was much greater than that observed with farnesol. Third, whereas the ability to block inactivated N-type channels was retained in DDA, its selectivity for N-type channels was lost.

Despite these differences, several qualitative features of farnesol block were also seen with DDA. For example, DDA block of L-type and non-L-type channels differed in its state-dependence. Like farnesol, DDA has the general ability to interact with multiple kinetic states of the channel. Finally, both farnesol and DDA accelerated the rate of

current decay and showed an increase in blocking affinity in lower concentrations of external barium in a manner consistent with an open channel blocking mechanism (Roullet et al., 1999). Nonetheless, whereas the general blocking mechanisms of farnesol are retained in the structurally much more rudimentary DDA molecule, many of the detailed aspects of calcium channel block by these two molecules appear quite distinct.

Effect of DDA on other membrane proteins

A wide diversity of biological actions of DDA have been reported in the literature, ranging from enhancement of skin permeation for drug delivery (Aungst et al., 1990) to inhibition of osmotic-sensitive calcium influx in bacteria (Beeler et al., 1997). However, DDA is perhaps best known as an inhibitor of the cardiac sodium/calcium exchanger. Philipson (1984) demonstrated ~60% inhibition of Na^+-dependent Ca^{2+} uptake by the canine cardiac Na^+/Ca^{2+} exchanger with 20 μM DDA, while a K_i of 3 μM has been reported for DDA inhibition of frog atrial "creep" currents, the electrogenic current generated by Na^+/Ca^{2+} exchange (Bielefeld et al., 1986). Consistent with our data on L-type channels ($IC_{50} \sim 0.8 \mu$M), Bielefeld reported that blocking affinity for myocardial L-type calcium and potassium currents occurred within the same range as block of exchange activity. In contrast, Terrar and White (1989) argued that DDA effects on cardiac calcium channels were only minimal compared to inhibition of Na^+/Ca^{2+} exchange. Our results obtained with N-type channels in 2 mM external barium (IC_{50} of 400 nM), together with the added inactivated channel block that would be present at a typical neuronal resting membrane potential, suggest that calcium channels may be much more sensitive to DDA than other ion transport molecules. Nonetheless, the observation that DDA is capable of inhibiting multiple types of cation transport proteins might reflect a common blocking mechanism. Based on the dependence of blocking affinity on external carrier ion concentration, one likely site of action of DDA is in the channel pore. Many types of cation channels share a similar P-loop motif, thus providing ample opportunity for conserved structures that may form the receptor site for DDA and related compounds. Consistent with such a mechanism, a number of monoamines have been shown to block inward rectifier potassium channels (Pearson and Nichols, 1998), and several of the structurally related quaternary ammonium compounds are potent pore blockers of voltage-dependent sodium channels (Wang et al., 1991).

Drug-structural requirements for N-type channel block

Several hydrocarbon molecules with different functional headgroups have been shown to block calcium channels.

For example, acidic omega-3 fatty acids (Leaf, 1995) have been reported to potently inhibit L-type calcium channels. In addition, compounds such as farnesol (Roullet et al., 1999) and aliphatic alcohols (Hawthorn et al., 1992) block calcium channels at micromolar concentrations. Therefore, one might expect the functional group to be relatively unimportant. Our finding that 1-dodecanol, n-dodecane, 4-dodecylphenol, and dodecylacetate show ~15% block at 10 μM would have been consistent with this idea. However, addition of a terminal amine (as in DDA) resulted in an almost 30-fold increase in blocking affinity compared with these other compounds. Thus, the functional group can be a major determinant of blocking efficacy of aliphatic monoamines. Additional structural derivatives will ultimately need to be examined to assess whether the addition of an amine group can generally enhance the blocking affinity of carbon chain molecules for calcium channels.

When comparing the effects of 1-dodecanol, DDA, and farnesol on steady-state inactivation of N-type channels, we can draw two conclusions. Compared with DDA, 1-dodecanol required 10-fold higher concentrations to mediate the same shift in half-inactivation potential, suggesting that the functional group contributes to the affinity for inactivated channels. Furthermore, farnesol, which carries the same functional group as 1-dodecanol, was 100-fold more effective in shifting the half-inactivation potential, strongly suggesting that the nature of the backbone structure is also critical for inactivated channel block.

We also observed a very sharp dependence of blocking affinity on hydrocarbon chain length for a series of aliphatic monoamines, with C12 and C13 compounds being most effective. While we cannot completely rule out the possibility that the longer molecules show a reduced degree of solubility, the reduced affinity seen with the longer compounds could also indicate that the blockers become too large to be properly accommodated by the binding site. Conversely, the lower blocking affinity observed with the shorter compounds could reflect an inability of these compounds to fully interact with all of the "microsites" contained within the overall drug-binding pocket on the channel. The dependence of blocking affinity on hydrocarbon chain length is not unique to voltage-dependent calcium channels. Experiments on inward rectifier K^+ channels revealed voltage-dependent block by monoamines that showed increasing potency and slower unblocking rates as the chain length was progressively increased from C5 to C12 (Pearson and Nichols, 1998). For open channel block of batrachotoxin-activated sodium channels by quaternary amines, increasing the side chain length from 12 to 18 carbons mediated an increase in mean blocked time (Wang et al., 1991). Furthermore, the authors identified a bell-shaped relation between blocking kinetics and carbon chain length. Philipson (1984) tested several aliphatic amines ranging from C8 to C16 (including DDA) and showed a progressively increasing potency for Na^+/Ca^{2+} exchange

inhibition. These data contrast with our finding that blocking affinity decreases as alkylamine chain length is increased past C13 and further differentiates the effects of alkylamines on Na$^+$/Ca^{2+} exchangers and Ca^{2+} channels. This may argue against the possibility that our observations with longer chain compounds are due to a simple solubility effect.

Mechanism of DDA block

Based on the observation that open channel block by farnesol seemed to require diffusion of the compound into the membrane phase, we had suggested that farnesol might perhaps act as a pore blocker from the cytoplasmic side of the channel (Roullet et al., 1999). Unlike farnesol, dodecylamine contains a tertiary amine with a pK$_a$ of 10.6, and thus DDA is essentially permanently charged at physiological pH and unavailable for crossing the plasma membrane. In several experiments, we added 10 μM DDA to the internal recording solution, and after 10 min of dialysis, we did not detect any significant block of N-type channels (Beedle and Zamponi, unpublished observations). Conversely, the rate constants for open channel block are three orders of magnitude faster than that required for equilibration of the drug, consistent with at least partial entry into the membrane phase rather than a simple pore occlusion mechanism from the external side of the channel. It is possible that the blocking site could be accessible via a membrane-delimited pathway similar to what has been proposed for lidocaine block of batrachotoxin-activated sodium channels (Zamponi et al., 1993a, b). If so, the terminal nitrogen moiety would remain confined to the extracellular side, whereas the hydrophobic tail end might access the actual blocking site. Such a mechanism could account for the observation that blocking affinity becomes reduced with decreasing carbon chain length and would space the drug binding site $\sim$10–15 Å into the lipid bilayer from the external side. However, how can such a model account for the observation that 1-dodecanol was only poorly effective in blocking N-type channel activity, despite sharing an identical backbone with DDA and being able to freely partition into the membrane phase? Clearly, the simple presence of the charged amino group dramatically enhances blocking affinity, but does not appear to be required for block (note that all of the compounds displayed in Fig. 1 show qualitatively similar block). It is conceivable that negative surface charges on the extracellular face of the membrane and/or the channel may serve to increase the local concentration of protonated DDA, thus resulting in an apparent increase in blocking affinity. The less effective surface charge screening associated with a reduction of the external divalent ion concentration would result in additional DDA accumulation near the membrane, thus providing a possible explanation for the higher DDA affinity for α_{1B} channels in lower ionic strength saline. However, the notion that this did not occur with L-type channels would argue against a diffuse membrane surface charge effect. Alternatively, the amino group of DDA could bind to one or more specific residues on the extracellular face of the channel protein, thereby facilitating the interaction between the hydrophobic tail and the functional blocking site on the channel. Ultimately, however, additional analogs such as quaternary derivatives will need to be examined to further substantiate our current hypothesis.

In summary, DDA is a remarkably simple compound capable of producing calcium channel block with submicromolar affinity. The observation that subtype specificity and blocking affinity of these carbon chain molecules can be dramatically altered with relatively small structural changes suggests that structural derivatives of this class of molecules may perhaps yield novel, high affinity blockers selective for certain types of voltage-dependent calcium channels.

REFERENCES

Aungst, B. J., J. A. Blake, and M. A. Hussain. 1990. Contributions of drug solubilization, partitioning, barrier disruption, and solvent permeation to the enhancement of skin permeation of various compounds with fatty acids and amines. *Pharm. Res.* 7:712–718.

Bangalore, R., N. Baindur, A. Rutledge, D. J. Trigle, and R. S. Kass. 1994. L-type calcium channels: asymmetrical intramembrane binding domain revealed by variable length, permanently charged 1,4-dihydropyridines. *Mol. Pharmacol.* 46:660–666.

Bech-Hansen, N. T., M. J. Naylor, T. A. Maybaum, W. G. Pearce, B. Koop, G. A. Fishman, M. Mets, M. A. Musarella, and K. M. Boycott. 1998. Loss-of-function mutations in a calcium-channel alpha1-subunit gene in Xp11.23 cause incomplete X-linked congenital stationary night blindness. *Nat. Genet.* 19:264–267.

Beeler, T., K. Gable, and T. Dunn. 1997. Activation of divalent cation influx into *S. cerevisiae* cells by hypotonic downshift. *J. Membr. Biol.* 160:77–83.

Bielefeld, D. R., R. W. Hadley, P. M. Vassilev, and J. R. Hume. 1986. Membrane electrical properties of vesicular Na-Ca exchange inhibitors in single atrial myocytes. *Circ. Res.* 59:381–389.

Boland, L. M., J. A. Morill, and B. P. Bean. 1994. ω-Conotoxin block of N-type calcium channels in frog and rat sympathetic neuron. *J. Neurosci.* 14:5011–5027.

Bourinet, E., T. W. Soong, K. Sutton, S. Slaymaker, E. Mathews, A. Monteil, G. W. Zamponi, J. Nargeot, and T. P. Snutch. 1999. Splicing of α_{1A} subunit gene generates phenotypic variants of P- and Q-type calcium channels. *Nature Neurosci.* 2:407–415.

Camm, A. J., H. A. Fozzard, M. J. Janse, R. Lazzara, M. R. Rosen, and P. J. Schwartz. 1991. The Sicilian gambit. A new approach to the classification of antiarrhythmic drugs based on their actions on arrhythmogenic mechanisms. *Circulation.* 84:1831–1851.

Catterall, W. A. 1991. Functional subunit structure of voltage-gated calcium channels. *Science.* 253:1499–1500.

Cribbs, L. L., J-H. Lee, J. Yang, J. Satin, Y. Zhang, A. Daud, J. Barclay, M. P. Williamson, M. Fox, M. Rees, and E. Perez-Reyes. 1998. Cloning and characterization of α_{1H} from human heart, a member of the T-type calcium channel gene family. *Circ. Res.* 83:103–109.

Dickson, C. T., A. R. Mena, and A. Alonso. 1997. Electroresponsiveness of medial entorhinal cortex layer III neurons in vitro. *Neuroscience.* 81:937–950.

Ellis, S. B., M. E. Williams, N. R. Ways, R. Brenner, A. H. Sharp, A. T. Leung, K. P. Campbell, E. McKenna, W. J. Koch, A. Hui, A. Schwartz, and M. M. Harpold. 1988. Sequence and expression of mRNAs encoding the α_1 and α_2 subunits of a DHP-sensitive calcium channel. *Science.* 241:1661–1664.

Fletcher, C. F., C. M. Lutz, T. N. O'Sullivan, J. D. Shaughnessy, Jr., R. Hawkes, W. N. Frankel, N. G. Copeland, and N. A. Jenkins. 1996. Absence epilepsy in tottering mutant mice is associated with calcium channel defects. *Cell.* 87:604–617.

Fox, J. A. 1995. Irreversible and reversible blockade of IMR32 calcium channel currents by synthetic MVIIA and iodinated MVIIC ω-conopeptides. *Pfluegers Arch.* 429:873–875.

Hawthorn, M. H., J. N. Ferrante, Y. W. Kwon, A. Rutledge, E. Luchowski, R. Bangalore, and D. J. Triggle. 1992. Effect of an homologous series of aliphatic alcohols on neuronal and smooth muscle voltage-dependent Ca^{2+} channels. *Eur. J. Pharmacol.* 229:143–148.

Higuchi, H., K. Nakano, C-H. Kim, B-S. Li, C-H. Kuo, E. Taira, and N. Miki. 1996. Ca^{2+}/calmodulin-dependent transcriptional activation of neuropeptide Y gene induced by membrane depolarization: determination of Ca^{2+} and cyclic AMP/phorbol 12-myristate 13-acetate-responsive elements. *J. Neurochem.* 66:1802–1809.

Leaf, A. 1995. Omega-3 fatty acids and prevention of ventricular fibrillation. *Prostaglandins Leukot. Essent. Fatty Acids.* 52:197–198.

Lee, J-H., A. N. Daud, L. L. Cribbs, A. E. Lacerdo, A. Pereverzev, U. Klöckner, T. Schneider, and E. Perez-Reyes. 1999. Cloning and expression of a novel member of the low voltage-activated T-type calcium channel family. *J. Neurosci.* 19:1912–1921.

Lemos, J. R., and M. C. Nowycky. 1989. Two types of calcium channels coexist in peptide-releasing vertebrate nerve terminals. *Neuron.* 2:1419–1426.

McCleskey, E. W. 1994. Calcium channels: cellular roles and molecular mechanisms. *Curr. Opin. Neurobiol.* 4:304–312.

Mintz, I. M., V. J. Venema, K. M. Swiderek, T. D. Lee, B. P. Bean, and M. E. Adams. 1992. P-type channels blocked by the spider toxin ω-Aga IVA. *Nature.* 355:827–829.

Ophoff, R. A., G. M. Terwindt, M. N. Vergouwe, R. van Eijk, P. J. Oefner, S. M. Hoffman, J. E. Lamerdin, H. W. Mohrenweiser, D. E. Bulman, M. D. Ferrari, and R. R. Frants. 1996. Familial hemiplegic migraine and episodic ataxia type-2 are caused by mutations in the Ca^{2+} channel gene CACNL1A4. *Cell.* 87:543–552.

Pearson, W. L., and C. G. Nichols. 1998. Block of Kir2.1 channel pore by alkylamine analogues of endogenous polyamines. *J. Gen. Physiol.* 112:351–363.

Perez-Reyes, E., L. L. Cribbs, A. Daud, A. E. Lacerdo, J. Barclay, M. P. Williamson, M. Fox, M. Rees, and J-H. Lee. 1998. Molecular characterization of neuronal low-voltage-activated T-type calcium channel. *Nature.* 391:896–900.

Philipson, K. D. 1984. Interaction of charged amphiphiles with Na^+-Ca^{2+} exchange in cardiac sarcolemmal vesicles. *J. Biol. Chem.* 259:13999–14002.

Roullet, J. B., R. L. Spaetgens, T. Burlingame, and G. W. Zamponi. 1999. Modulation of neuronal voltage-gated calcium channels by farnesol. *J. Biol. Chem.* 274:25439–25446.

Terrar, D. A., and E. White. 1989. Mechanisms and significance of calcium entry at positive membrane potentials in guinea-pig ventricular muscle cells. *Q. J. Exp. Physiol.* 74:121–139.

Tomlinson, W. J., A. Stea, E. Bourinet, P. Charnet, J. Nargeot, and T. P. Snutch. 1993. Functional properties of a neuronal class C L-type calcium channel. *Neuropharmacology.* 32:1117–1126.

Tsien, R. W., P. T. Ellinor, and W. A. Horne. 1991. Molecular diversity of voltage-dependent Ca^{2+} channels. *TINS.* 12:349–354.

Wang, G. K., R. Simon, and S. Y. Wang. 1991. Quaternary ammonium compounds as structural probes of single batrachotoxin-activated Na+ channels. *J. Gen. Physiol.* 98:1005–1024.

Williams, M. E., P. F. Brust, D. H. Feldman, S. Patthi, S. Simerson, A. Maroufi, A. F. McCue, G. Veliçelebi, S. B. Ellis, and M. M. Harpold. 1992a. Structure and functional expression of an ω-conotoxin-sensitive human N-type calcium channel. *Science.* 257:389–395.

Williams, M. E., D. H. Feldman, A. F. McCue, R. Brenner, G. Velicelebi, S. B. Ellis, and M. M. Harpold. 1992b. Structure and functional expression of α_1, α_2, and β subunits of a novel human neuronal calcium channel subtype. *Neuron.* 8:71–84.

Williams, M. E., L. M. Marubio, C. R. Deal, M. Hans, P. F. Brust, L. H. Philipson, R. J. Miller, E. C. Johnson, M. M. Harpold, and S. B. Ellis. 1994. Structure and functional characterization of neuronal α_{1E} calcium channel subtypes. *J. Biol. Chem.* 269:22347–22357.

Zamponi, G. W. 1997. Antagonist binding sites of voltage-dependent calcium channels. *Drug Dev. Res.* 42:131–143.

Zamponi, G. W., D. D. Doyle, and R. J. French. 1993a. Fast lidocaine block of cardiac and skeletal muscle sodium channels: one site with two routes of access. *Biophys. J.* 65:80–90.

Zamponi, G. W., D. D. Doyle, and R. J. French. 1993b. State-dependent block underlies the tissue specificity of lidocaine action on batracho-toxin-activated cardiac sodium channels. *Biophys. J.* 65:91–100.

Zhang, J.-F., A. D. Randall, P. T. Ellinor, W. A. Horne, W. A. Sather, T. Tanabe, T. L. Schwarz, and R. W. Tsien. 1993. Distinctive pharmacology and kinetics of cloned neuronal Ca^{2+} channels and their possible counterparts in mammalian CNS neurons. *Neuropharmacology.* 32:1075–1088.